



Electron-electron interaction and correlation-induced two density waves with different Fermi velocities in graphene quantum dots

Hui-Ying Ren, Ya-Ning Ren, Qi Zheng , Jia-Qi He, and Lin He ^{*}

Center for Advanced Quantum Studies, Department of Physics, Beijing Normal University, Beijing 100875, People's Republic of China and Key Laboratory of Multiscale Spin Physics, Ministry of Education, Beijing 100875, People's Republic of China



(Received 28 December 2022; accepted 10 August 2023; published 23 August 2023)

Graphene quantum dots (GQDs) can exhibit a range of spectacular phenomena such as the Klein tunneling induced quasibound states and Berry phase tuned energy spectra. According to previous studies, all these interesting quantum phenomena seem to be well understood in the free electron picture. However, electronic motion in the GQDs is locally reduced to quantized orbits by quantum confinement, which implies that the kinetic energy in the GQDs may be comparable to or even smaller than the Coulomb energy of the quasiparticles, possibly resulting in exotic correlated phases. Here we present a scanning tunneling microscopy and spectroscopy study of gate-tunable GQDs in graphene/WSe₂ heterostructure devices and report a correlation-induced exotic phase in the GQDs. Gating allows us to precisely characterize effects of the electron-electron interaction on the energy spectra of the GQDs. By measuring density of states as a function of energy and position, we explicitly uncover two density waves with different velocities in the GQDs, attributing to spin-charge separation in real space.

DOI: [10.1103/PhysRevB.108.L081408](https://doi.org/10.1103/PhysRevB.108.L081408)

Exotic many-body quantum phases often occur in systems with strong electron-electron (e - e) interactions [1–5]. Creating a flat band is a well-established method to realize strongly correlated systems, in which the e - e interactions U can largely exceed the kinetic energy of electrons set by the bandwidth W . Therefore, significant efforts have been devoted to the search for emergent quantum phenomena in Landau levels and moiré flat bands. These studies have achieved great success and many exotic correlated phases have been observed [1–5].

Recent advances in introducing quantum confinement in a continuous graphene system have provided a route to strongly suppressing the kinetic energy of quasiparticles [6–25], as schematically shown in Fig. 1(a). In graphene quantum dots (GQDs), electronic motion is locally reduced to quantized quasibound states by quantum confinement, i.e., the Klein tunneling induced whispering gallery mode (WGM) [6–11], implying that the e - e interactions should play an important role in determining their electronic properties. However, almost all the interesting quantum phenomena reported in the GQDs can be well understood in the free electron picture [6–25]. Although some spectroscopic evidence of e - e interactions in the GQDs has been observed, clear identification of e - e interactions on the energy spectra is still missing due to the metallic substrate and the lack of gate control [26]. In this Letter, we report the observation of e - e interactions and a correlation-induced exotic phase in the GQDs. Our gate-tunable devices enable unambiguous measurement of effects of the e - e interactions on the energy spectra of the GQDs. The e - e interactions and the suppressed quantum kinetic energy lead to a correlated phase in the GQDs: two density waves

with different velocities, attributing to spin-charge separation in real space, are explicitly uncovered.

Figure 1(b) shows a schematic of the experimental device setup of a GQD embedded in gate-tunable graphene/WSe₂ heterostructure devices. In our experiment, a nanoscale 1T'-phase monolayer WSe₂ island is created on top of a 2H-phase WSe₂ substrate, as shown in Fig. 1(c), to introduce electrostatic potential on the graphene above it. The 1T'-phase monolayer WSe₂ island generates the GQD to confine massless Dirac fermions of graphene, which is the reason we use WSe₂ as the substrate in this work [11,27,28] (see Fig. S1 and the Supplemental Material for details [29]). Figure 1(d) shows typical scanning tunneling spectroscopy (STS), i.e., dI/dV , spectroscopic map across the GQD and a sequence of temporarily confined quasibound states can be clearly observed. At the edge of a GQD, the quasibound states are generated by the Klein tunneling induced WGM and they are almost equally spaced in energy (see Figs. S2 and S3 [29]) [6–13]. For a circular GQD with the size of confined region L , the energy spacing E_0 between the quasibound states should be described by $\Delta E \approx 2\hbar v_F/L$, where \hbar is the reduced Planck's constant and v_F is the Fermi velocity. In Fig. 1(e), we summarize the energy spacing from nine GQDs with different sizes observed in our experiment. Here, only the STS spectra recorded along the long-axis direction of the GQDs are analyzed because, usually, we can obtain several well-defined quasibound states confined along this axis. Only the GQDs that have two quasibound states flanking the Fermi level are selected. Fitting the data yields the Fermi velocity $v_F \approx 1.2 \times 10^6$ m/s, further confirming the confinement of the massless Dirac fermions in the GQDs.

A notable feature observed in our experiment is that the energy spacing between the two quasibound states flanking the Fermi level (i.e., the highest occupied and the lowest

^{*}helin@bnu.edu.cn

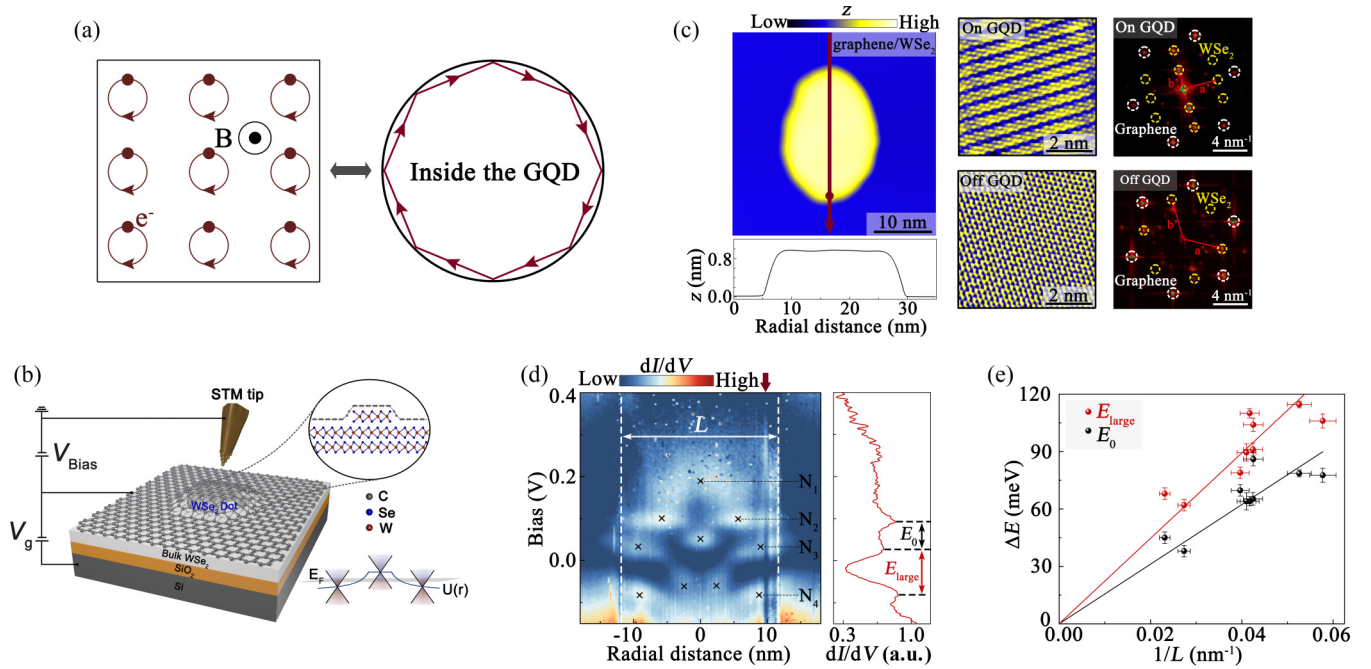


FIG. 1. STM characterization of GQDs. (a) Left panel: Schematic of cyclotron motion of electrons under a magnetic field. Right panel: Schematic of a circular GQD with a typical closed interference path of trapping quasiparticles. (b) Schematic of the experimental device setup. (c) Top left panel: STM topography of a typical GQD ($V_b = 700$ mV, $I_{set} = 100$ pA). Bottom left panel: Profile line of the GQD showing the height ~ 0.8 nm. Middle panels: Enlarged STM images on ($V_b = 200$ mV, $I_{set} = 200$ pA) and off ($V_b = 400$ mV, $I_{set} = 100$ pA), a representative GQD, respectively. Right panels: The fast Fourier transform (FFT) images obtained from the STM images in the middle panels. The white circles show reciprocal lattices of graphene. The yellow circles show reciprocal lattices of WSe_2 . The red arrows show the reciprocal lattice vectors a' and b' of WSe_2 . The unlabeled bright spots correspond to the reciprocal moiré superlattices and higher-order scattering. (d) Left panel: A radially dI/dV spectroscopic map along the arrow in panel (c). The black crosses indicate the quasibound states, and the two white dashed lines mark the size of confined region L . Right panel: A dI/dV spectrum recorded at the position indicated by the red arrow in the left panels, corresponding to the real-space location indicated by a red solid dot in panel (c). (e) Measured large (red) and normal (black) energy separations for the GQDs of different sizes. Both of them scale as $1/L$. The straight lines represent linear fits to the data.

unoccupied quasibound states), labeled as E_{large} , is much larger than E_0 (E_0 is the energy spacing between the two quasibound states that are both at one side of the Fermi level), as shown in Fig. 1(d) (see Fig. S3 for more experimental results [29]). Similar results have been observed in the two flat bands of magic-angle twisted bilayer graphene (MATBG) [30–33] and in quantized confined states of finite-size Tomonaga-Luttinger liquids (TLLs) [34–36]. Both the energy separation between the two flat bands in the MATBG and the energy difference between the two confined states in the finite-size TLLs are much larger when they are flanking the Fermi level; they are clear signatures of the e - e interactions [30–36]. In the GQDs, the energy difference between the E_{large} and the E_0 directly reflects the e - e interaction strength E_C , i.e., $E_{\text{large}} \approx E_0 + E_C$. The Coulomb energy E_C of two electrons should be inversely proportional to their separation L , i.e., E_C is expected to scale as L^{-1} . Therefore, the E_{large} should also be inversely proportional to L , as demonstrated explicitly in our experiment [Fig. 1(e)].

To further explore the e - e interactions on the energy spectra of the GQDs, we perform STS measurement of the GQDs for different gate voltages. Figure 2(a) shows the gate-dependent dI/dV curves acquired at a GQD with $L \approx 19$ nm. A key observation is that the energy separation between the two peaks flanking the Fermi level changes with

gate voltage. Two representative STS spectra at $V_g = 18$ V and $V_g = -4$ V are plotted in Fig. 2(b). At $V_g = 18$ V, the energy separation between the N_2 and N_3 states, the E_{large} , is about 115 meV, which is larger than the $E_0 \sim 79$ meV between the N_1 (N_3) and N_2 (N_4) states. For $V_g = -4$ V, the N_3 state is nearly half filled and is split into two peaks, the N_{3+} and N_{3-} , with reduced intensities. Then the energy separation between the N_{3+} and N_{3-} , i.e., the E_C , is about 35 meV. Such a measurement demonstrates explicitly that $E_{\text{large}} \approx E_0 + E_C$ (see Fig. S4 for more gate-dependent measurements on the other GQD; the same result can be obtained [29]). The observed gate-induced modulation of the energy spectra reveals that e - e interaction plays an important role in determining the electronic properties of the GQDs. When e - e interaction is absent, as schematically shown in Fig. 2(c) (left panel), the energy separation between the quasibound states would be gate and energy independent and should be equal to the single-particle level spacing value in a box (see Fig. S5 for theoretical spectra in the GQDs without considering the e - e interaction [29]). The presence of e - e interaction, Fig. 2(c) (right panel), explains well the large and small energy separations observed for different energies (results in Fig. 1) and different electron fillings (results in Fig. 2). The splitting of the half-filled quasibound state may arise from the lifting of spin degeneracy by

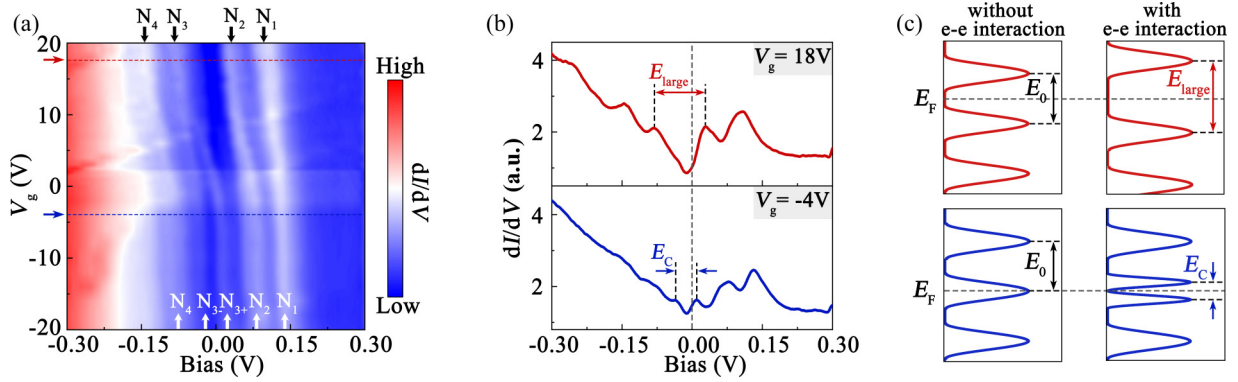


FIG. 2. Gate-dependent electronic structure of the GQD. (a) A density plot of dI/dV spectra acquired for $-20 \text{ V} \leq V_g \leq 20 \text{ V}$ on the GQD showing the energy separation transition as a function of V_g (set-point parameters: $V_b = 700 \text{ mV}$, $I_{\text{set}} = 300 \text{ pA}$). The black or white arrows indicate the resonance peaks arising from the quasibound states. (b) Two typical dI/dV spectra at $V_g = 18$ and -4 V , respectively, which are marked with the arrows in (a). The N_3 state splits into two peaks with different intensities when it is near half filled. (c) Quasibound-state diagram for the energy separation without (left panels) and with (right panels) $e-e$ interactions.

the strong Coulomb interaction [37–39], or may arise from a correlation-induced Mott-Hubbard transition [1–5,30–33]. Further experiments should be carried out to explore its exact nature.

In the GQDs, the $e-e$ interaction is about several tens of millielectron volts and is comparable to the full width at half maximum of the quasibound states (results in Figs. 1 and 2), possibly causing correlation physics to manifest experimentally by the emergence of new quantum states. To further explore correlated phases in the GQDs, we measure the dI/dV spectra of a GQD and perform Fourier transform (FT) analysis of the resulting density plot, as summarized in Figs. 3(a)–3(c). Here we choose such a GQD [Fig. 3(a)] because the quasi-one-dimensional confinement along the long side much simplifies the analysis of real-space standing waves of the confined quasiparticles. Moreover, a longer confinement also allows us to achieve better momentum resolution. Figure 3(b) shows the STS intensity plot as a function of position (x axis) along the arrow in Fig. 3(a) and the sample bias (y axis), which directly reflects real-space modulation of the local density of states (LDOS) at different energies. The number of nodal points of the LDOS increases with changing the energies away from the Dirac point (at about 246 meV in the GQD). The corresponding FT of the STS intensity plot, as shown in Fig. 3(c), directly reveals the dispersion of the quasibound states in the GQD. Unexpectedly, two linear dispersion branches with different velocities, $v_{F1} \approx 1.09 \times 10^6 \text{ m/s}$ and $v_{F2} \approx 1.36 \times 10^6 \text{ m/s}$, are seen to cross the Dirac point (see the Supplemental Material for details of the fitting in determining the Fermi velocities and Fig. S6 for more experimental data [29]). Such a result is quite different from the expected result in the free electron picture, i.e., a density wave with one velocity, as schematically shown in the top panel of Fig. 3(d) (see Fig. S7 for the theoretical result of one-dimensional (1D) confinement without considering the $e-e$ interaction [29]).

The existence of two density waves with different velocities in the GQD is further confirmed by carrying out STS mappings, which directly reflect the LDOS in real space at the selected energies. In a quantum confined system with a fixed size, the two density waves with different velocities will form the standing waves at different discrete energies,

which provide characteristic fingerprints in the scanning tunneling microscope (STM) measurement. Figure 4(a) shows representative STS maps measured at five different energies of the GQD in Fig. 3(a). Figure 4(b) shows typical profile lines of the five STS maps and the values of the profile lines at the boundaries of the confined potential are shifted to zero for comparison. The corresponding pattern expected for free particles with $v_{F2} \approx 1.36 \times 10^6 \text{ m/s}$ and the Dirac point $E_D \approx 246 \text{ meV}$ is confined to a 1D box of the same length is shown in Fig. 4(c). Three significant discrepancies are present compared to Fig. 4(c): In the experiment (1) the number of maxima in the DOS at 30 meV is four; (2) the minimum between two maxima in the DOS is much larger than zero at 115 and 30 meV; (3) the spatial separation between two adjacent maxima is not approximately equidistant at 30 meV. These discrepancies can be naturally explained by considering the existence of two density waves with different velocities and the correlation-induced large energy separation of the quasibound states around the Fermi level. Figure 4(d) shows the DOSs at different energies by superposition of two density waves with $v_{F1} \approx 1.09 \times 10^6 \text{ m/s}$, $v_{F2} \approx 1.36 \times 10^6 \text{ m/s}$, and the Dirac point $E_D \approx 246 \text{ meV}$ [determined experimentally in Fig. 3(c)], which reproduce well the main features observed in our experiment (see the Supplemental Material for further discussion [29]).

With considering two intrinsic properties of electrons, i.e., the charge and spin, the correlation-induced two density waves with different velocities in the GQDs are reasonably attributed to spin- and charge-density waves. The two dispersions with different velocities also remind us of the spin-charge separation induced by $e-e$ interactions in the TLLs [34–37,40,41]. The linear dispersion branch with smaller Fermi velocity, which is attributed to the spin-density wave, is consistent with the expected Fermi velocities in a graphene monolayer [42,43]. The other linear dispersion branch with larger Fermi velocity is attributed to the charge-density wave. However, we should point out that the spin-charge separation observed in the GQDs is quite different from that in the TLLs. First, the ratio between the velocities for the spin- and charge-density waves v_{F1}/v_{F2} in the GQDs is about $\sim 0.75 \pm 0.05$, which is larger than that, $\sim 0.53 \pm 0.05$,

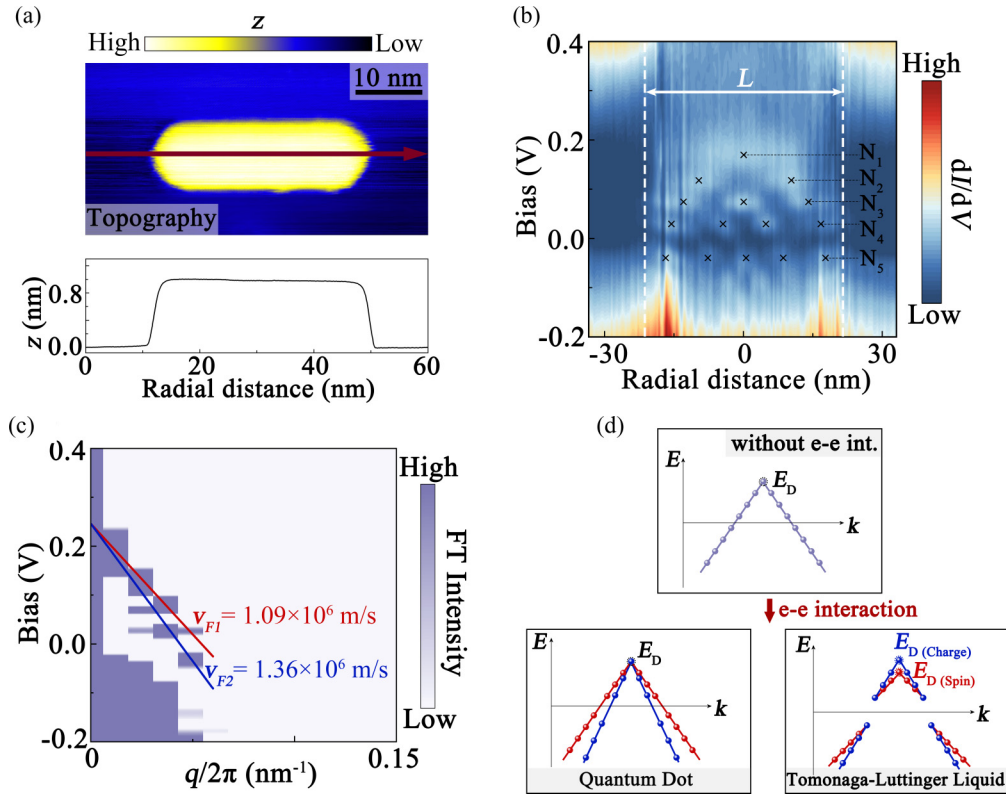


FIG. 3. Dispersion of quasibound states in a GQD. (a) Top panel: STM topography of a typical GQD (set-point parameters: $V_b = 600$ mV, $I_{\text{set}} = 100$ pA). Bottom panel: Profile line chart along the red straight line with an arrow in the top panel. (b) A radially dI/dV spectroscopic map along the red straight line with an arrow in (a). The black crosses indicate the quasibound states, and the two white dashed lines mark the size of the confined region. The position of the Dirac point E_D is ~ 246 meV and the size of the confined region L is ~ 43.3 nm. (c) FT of the dI/dV data in (b) as a function of bias voltage V_b and wave vector q . Two linear dispersion branches with different velocities (marked in red and blue) are observed. (d) Schematic diagram of dispersion in a quasi one-dimensional GQD. Top panel: dispersion in the GQD without $e-e$ interactions. Bottom left panel: dispersion in the GQD with $e-e$ interactions. There are two density waves with different velocities. Bottom right panel: spin-charge separation in the Tomonaga-Luttinger liquids.

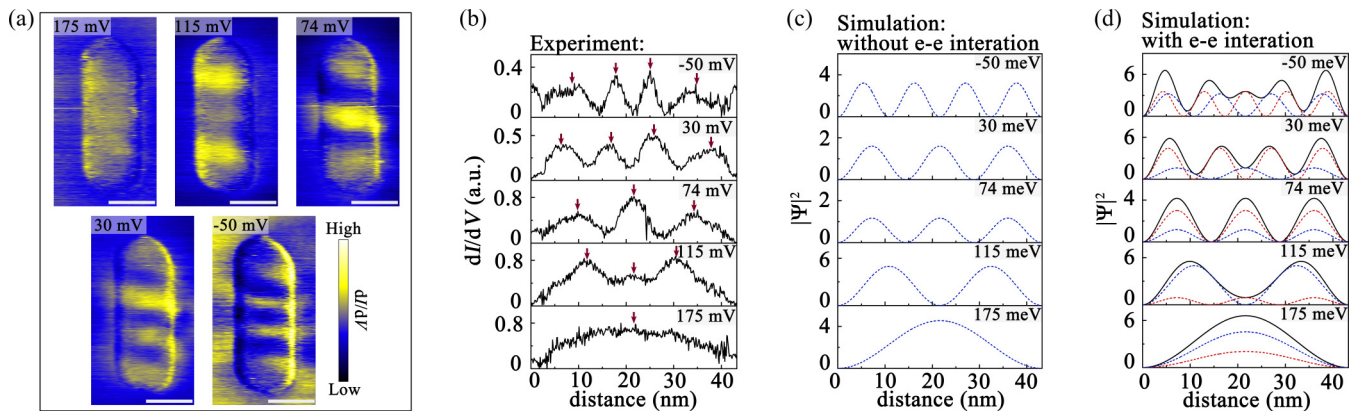


FIG. 4. Imaging two density waves with different velocities in real space. (a) Representative STS maps recorded at different energies of the GQD in Fig. 3(a). Standing waves with different number of maxima in the DOS are formed at different energies due to the quantum confinement. (b) Typical profile lines of the five STS maps in (a) with the size of confined region $L \approx 43.3$ nm. (c) Theoretical LDOS assuming noninteracting quasiparticles with the Fermi velocity 1.36×10^6 m/s and the Dirac point $E_D = 246$ meV confined in a one-dimensional box with $L \approx 43.3$ nm. (d) Theoretical LDOS by considering the confinement of two density waves with different velocities, $v_{F1} = 1.09 \times 10^6$ m/s, $v_{F2} = 1.36 \times 10^6$ m/s, and the Dirac point $E_D = 246$ meV confined in a one-dimensional box with $L \approx 43.3$ nm. The correlation-induced large energy separation of the quasibound states around the Fermi level is considered in the simulation. Scale bar: 10 nm in (a).

observed in the finite-size TLLs very recently [34], possibly due to the relatively weaker e - e interactions in the GQDs. Second, as schematically sketched in Fig. 3(d), the highest occupied and the lowest unoccupied states in the TLLs are the so-called zero modes; i.e., no spin or charge modes are excited [34–37]. Injecting electrons or holes into the TLLs will create spin and charge excitations with different velocities [Fig. 3(d), right bottom panel]. In the GQDs, the correlation-induced spin- and charge-density waves with different velocities emerge for all the temporarily confined quasiparticles, i.e., for all the quasiparticles below the Dirac point [Fig. 3(d), left bottom panel]. The differences uncovered highlight the need for further theoretical developments and an alternative theory with different mechanism of the TLLs should be constructed to fully understand the correlation-induced spin-charge separation in the GQDs.

In summary, the effects of the e - e interactions on the energy spectra of the GQDs are unambiguously measured in our gate-tunable devices. In the GQDs, two density waves with different velocities, attributed to spin-charge separation

in real space, are explicitly uncovered. These interesting phenomena cannot be explained in the absence of e - e interactions and highlight the importance of correlations in the GQDs. Our result suggests that the spin-charge separation may be a universal ground state in finite-size systems, such as TLLs and GQDs, with strong correlated effects. Further theoretical and experimental work is necessary to fully ascertain the importance of correlation effects in the GQDs.

We thank Professor Qing-Feng Sun and Yu-Chen Zhuang at Peking University for helpful discussion. This work was supported by the National Key R and D Program of China (Grants No. 2021YFA1400100 and No. 2021YFA1401900), National Natural Science Foundation of China (Grants No. 12141401 and No. 11974050), and “the Fundamental Research Funds for the Central Universities.” The devices were fabricated using the transfer platform from Shanghai Onway Technology Co., Ltd.

H.-Y.R., Y.-N.R, and Q.Z. contributed equally to this work.

-
- [1] V. N. Kotov, B. Uchoa, V. M. Pereira, F. Guinea, and A. H. Castro Neto, Electron-electron interactions in graphene: Current status and perspectives, *Rev. Mod. Phys.* **84**, 1067 (2012).
- [2] L. Balents, C. R. Dean, D. K. Efetov, and A. F. Young, Superconductivity and strong correlations in moiré flat bands, *Nat. Phys.* **16**, 725 (2020).
- [3] E. Y. Andrei and A. H. MacDonald, Graphene bilayers with a twist, *Nat. Mater.* **19**, 1265 (2020).
- [4] Y.-N. Ren, Y. Zhang, Y.-W. Liu, and L. He, Twistronics in graphene-based van der Waals structures, *Chin. Phys. B* **29**, 117303 (2020).
- [5] C. N. Lau, M. W. Bockrath, K. F. Mak, and F. Zhang, Reproducibility in the fabrication and physics of moiré materials, *Nature (London)* **602**, 41 (2022).
- [6] S.-Y. Li and L. He, Recent progresses of quantum confinement in graphene quantum dots, *Front. Phys.* **17**, 33201 (2021).
- [7] Y. Zhao, J. Wyrick, F. D. Natterer, J. F. Rodriguez-Nieva, C. Lewandowski, K. Watanabe, T. Taniguchi, L. S. Levitov, N. B. Zhitenev, and J. A. Stroscio, Creating and probing electron whispering-gallery modes in graphene, *Science* **348**, 672 (2015).
- [8] C. Gutiérrez, L. Brown, C.-J. Kim, J. Park, and A. N. Pasupathy, Klein tunnelling and electron trapping in nanometre-scale graphene quantum dots, *Nat. Phys.* **12**, 1069 (2016).
- [9] J. Lee, D. Wong, J. Velasco, Jr., J. F. Rodriguez-Nieva, S. Kahn, H.-Z. Tsai, T. Taniguchi, K. Watanabe, A. Zettl, F. Wang, L. S. Levitov, and M. F. Crommie, Imaging electrostatically confined Dirac fermions in graphene quantum dots, *Nat. Phys.* **12**, 1032 (2016).
- [10] Z.-Q. Fu, Y. Pan, J.-J. Zhou, K.-K. Bai, D.-L. Ma, Y. Zhuang, J.-B. Qiao, H. Jiang, H. Liu, and L. He, Relativistic artificial molecules realized by two coupled graphene quantum dots, *Nano Lett.* **20**, 6738 (2020).
- [11] Q. Zheng, Y.-C. Zhuang, Q.-F. Sun, and L. He, Coexistence of electron whispering-gallery modes and atomic collapse states in graphene/WSe₂ heterostructure quantum dots, *Nat. Commun.* **13**, 1597 (2022).
- [12] F. Ghahari, D. Walkup, C. Gutierrez, J. F. Rodriguez-Nieva, Y. Zhao, J. Wyrick, F. D. Natterer, W. G. Cullen, K. Watanabe, T. Taniguchi, L. S. Levitov, N. B. Zhitenev, and J. A. Stroscio, An on/off Berry phase switch in circular graphene resonators, *Science* **356**, 845 (2017).
- [13] Z.-Q. Fu, Y. Zhang, J.-B. Qiao, D.-L. Ma, H. Liu, Z.-H. Guo, Y.-C. Wei, J.-Y. Hu, Q. Xiao, X.-R. Mao, and L. He, Spatial confinement, magnetic localization, and their interactions on massless Dirac fermions, *Phys. Rev. B* **98**, 241401 (2018).
- [14] Y.-N. Ren, Q. Cheng, S.-Y. Li, C. Yan, Y.-W. Liu, K. Lv, M.-H. Zhang, Q.-F. Sun, and L. He, Spatial and magnetic confinement of massless Dirac fermions, *Phys. Rev. B* **104**, L161408 (2021).
- [15] M. Eich, F. Herman, R. Pisoni, H. Overweg, A. Kurzmam, Y. Lee, P. Rickhaus, K. Watanabe, T. Taniguchi, M. Sigrist, T. Ihn, and K. Ensslin, Spin and Valley States in Gate-Defined Bilayer Graphene Quantum Dots, *Phys. Rev. X* **8**, 031023 (2018).
- [16] A. Kurzmam, M. Eich, H. Overweg, M. Mangold, F. Herman, P. Rickhaus, R. Pisoni, Y. Lee, R. Garreis, C. Tong, K. Watanabe, T. Taniguchi, K. Ensslin, and T. Ihn, Excited States in Bilayer Graphene Quantum Dots, *Phys. Rev. Lett.* **123**, 026803 (2019).
- [17] Y.-W. Liu, Z. Hou, S.-Y. Li, Q.-F. Sun, and L. He, Movable Valley Switch Driven by Berry Phase in Bilayer-Graphene Resonators, *Phys. Rev. Lett.* **124**, 166801 (2020).
- [18] L. Banszerus, A. Rothstein, T. Fabian, S. Moller, E. Icking, S. Trellenkamp, F. Lentz, D. Neumaier, K. Watanabe, T. Taniguchi, F. Libisch, C. Volk, and C. Stampfer, Electron-hole crossover in gate-controlled bilayer graphene quantum dots, *Nano Lett.* **20**, 7709 (2020).
- [19] C. Tong, R. Garreis, A. Knothe, M. Eich, A. Sacchi, K. Watanabe, T. Taniguchi, V. Fal’ko, T. Ihn, K. Ensslin, and A. Kurzmam, Tunable valley splitting and bipolar operation in graphene quantum dots, *Nano Lett.* **21**, 1068 (2021).

- [20] Y.-N. Ren, Q. Cheng, Q.-F. Sun, and L. He, Realizing Valley-Polarized Energy Spectra in Bilayer Graphene Quantum Dots via Continuously Tunable Berry Phases, *Phys. Rev. Lett.* **128**, 206805 (2022).
- [21] M. I. Katsnelson, K. S. Novoselov, and A. K. Geim, Chiral tunnelling and the Klein paradox in graphene, *Nat. Phys.* **2**, 620 (2006).
- [22] K.-K. Bai, J.-B. Qiao, H. Jiang, H. Liu, and L. He, Massless Dirac fermions trapping in a quasi-one-dimensional n - p - n junction of a continuous graphene monolayer, *Phys. Rev. B* **95**, 201406 (2017).
- [23] C. W. J. Beenakker, Colloquium: Andreev reflection and Klein tunneling in graphene, *Rev. Mod. Phys.* **80**, 1337 (2008).
- [24] K.-K. Bai, J.-J. Zhou, Y.-C. Wei, J.-B. Qiao, Y.-W. Liu, H.-W. Liu, H. Jiang, and L. He, Generating atomically sharp p - n junctions in graphene and testing quantum electron optics on the nanoscale, *Phys. Rev. B* **97**, 045413 (2018).
- [25] Y.-N. Ren, Y.-C. Zhuang, Q.-F. Sun, and L. He, Magnetic Field-Tunable Valley-Contrasting Pseudomagnetic Confinement in Graphene, *Phys. Rev. Lett.* **129**, 076802 (2022).
- [26] Z.-Q. Fu, K.-K. Bai, Y.-N. Ren, J.-J. Zhou, and L. He, Coulomb interaction in quasibound states of graphene quantum dots, *Phys. Rev. B* **101**, 235310 (2020).
- [27] Q. Zheng, Y.-C. Zhuang, Y.-N. Ren, C. Yan, Q.-F. Sun, and L. He, Molecular Collapse States in Graphene/WSe₂ Heterostructure Quantum Dots, *Phys. Rev. Lett.* **130**, 076202 (2023).
- [28] Y.-N. Ren, M.-H. Zhang, Q. Zheng, and L. He, Tailoring interfacial nanostructures at graphene/transition metal dichalcogenide heterostructures, [arXiv:2212.01774](https://arxiv.org/abs/2212.01774).
- [29] See Supplemental Material at <http://link.aps.org/supplemental/10.1103/PhysRevB.108.L081408> for more experimental data, theoretical calculation, analysis, and further discussion,
- [30] Y. Xie, B. Lian, B. Jack, X. Liu, C. L. Chiu, K. Watanabe, T. Taniguchi, B. A. Bernevig, and A. Yazdani, Spectroscopic signatures of many-body correlations in magic-angle twisted bilayer graphene, *Nature (London)* **572**, 101 (2019).
- [31] A. Kerelsky, L. J. McGilly, D. M. Kennes, L. Xian, M. Yankowitz, S. Chen, K. Watanabe, T. Taniguchi, J. Hone, C. Dean, A. Rubio, and A. N. Pasupathy, Maximized electron interactions at the magic angle in twisted bilayer graphene, *Nature (London)* **572**, 95 (2019).
- [32] Y. Jiang, X. Lai, K. Watanabe, T. Taniguchi, K. Haule, J. Mao, and E. Y. Andrei, Charge order and broken rotational symmetry in magic-angle twisted bilayer graphene, *Nature (London)* **573**, 91 (2019).
- [33] Y. Choi, J. Kemmer, Y. Peng, A. Thomson, H. Arora, R. Polski, Y. Zhang, H. Ren, J. Alicea, G. Refael, F. van Oppen, K. Watanabe, and T. Taniguchi, S. Nadj-Perge, Electronic correlations in twisted bilayer graphene near the magic angle, *Nat. Phys.* **15**, 1174 (2019).
- [34] T. Zhu, W. Ruan, Y.-Q. Wang, H.-Z. Tsai, S. Wang, C. Zhang, T. Wang, F. Liou, K. Watanabe, T. Taniguchi, J. B. Neaton, A. Weber-Bargioni, A. Zettl, Z.-Q. Qiu, G. Zhang, F. Wang, J. E. Moore, and M. F. Crommie, Imaging gate-tunable Tomonaga-Luttinger liquids in 1H-MoSe₂ mirror twin boundaries, *Nat. Mater.* **21**, 748 (2022).
- [35] W. Jolie, C. Murray, P. S. Weiß, J. Hall, F. Portner, N. Atodiresei, A. V. Krasheninnikov, C. Busse, H.-P. Komsa, A. Rosch, and T. Michely, Tomonaga-Luttinger Liquid in a Box: Electrons Confined within MoS₂ Mirror-Twin Boundaries, *Phys. Rev. X* **9**, 011055 (2019).
- [36] X. Yang, Z.-L. Gu, H. Wang, J.-J. Xian, S. Meng, N. Nagaosa, W.-H. Zhang, H.-W. Liu, Z.-H. Ling, K. Fan, Z.-M. Zhang, L. Qin, Z.-H. Zhang, Y. Liang, J.-X. Li, and Y.-S. Fu, Manipulating Hubbard-type Coulomb blockade effect of metallic wires embedded in an insulator, *Natl. Sci. Rev.* **10**, nwac210 (2023).
- [37] C. Efferen, J. Fischer, A. Rosch, T. Michely, and W. Jolie, Modulated Kondo screening along magnetic mirror twin boundaries in monolayer MoS₂ on graphene, [arXiv:2210.09675](https://arxiv.org/abs/2210.09675).
- [38] H. Gonzalez-Herrero, J. M. Gomez-Rodriguez, P. Mallet, M. Moaied, J. J. Palacios, C. Salgado, M. M. Ugeda, J.-Y. Veullen, F. Yndurain, and I. Brihuela, Atomic-scale control of graphene magnetism by using hydrogen atoms, *Science* **352**, 437, (2016).
- [39] Y. Zhang, S.-Y. Li, H. Huang, W.-T. Li, J. B. Qiao, W.-X. Wang, L.-J. Yin, W.-H. Duan, and L. He, Scanning Tunneling Microscopy of the Π Magnetism of a Single Carbon Vacancy in Graphene, *Phys. Rev. Lett.* **117**, 166801 (2016).
- [40] S.-I. Tomonaga, Remarks on Bloch's method of sound waves applied to many-fermion problems, *Prog. Theor. Phys.* **5**, 544 (1950).
- [41] J. M. Luttinger, An exactly soluble model of a many-fermion system, *J. Math. Phys. (NY)* **4**, 1154 (1963).
- [42] L.-J. Yin, K.-K. Bai, W.-X. Wang, S.-Y. Li, Y. Zhang, and L. He, Landau quantization of Dirac fermions in graphene and its multilayers, *Front. Phys.* **12**, 127408 (2017).
- [43] K.-K. Bai, Y.-C. Wei, J.-B. Qiao, S.-Y. Li, L.-J. Yin, W. Yan, J.-C. Nie, and L. He, Detecting giant electron-hole asymmetry in graphene monolayer generated by strain and charge-defect scattering via Landau level spectroscopy, *Phys. Rev. B* **92**, 121405(R) (2015).